Peer-reviewed version available at Appl. Sci. 2019, 9, 2279; doi:10.3390/app9112279

Article

Carrier dynamics in InGaN/GaN on the basis of different In concentrations

Zhi Ting Ye,[1] Hong Thai Nguyen,[2] Shih-Wei Feng,[3] Hsiang-Chen Wang,[2,*] and Hwei-Ling Chou[4,*]

[1] Department of Electro-Optical Engineering, National United University, 2, Lienda, Miaoli 26063, Taiwan; ztye@nuu.edu.tw;
[2] Graduate Institute of Opto-Mechatronics and Advanced Institute of Manufacturing with High-Tech Innovations (AIM-HI), National Chung Cheng University, Chia-Yi 62102, Taiwan; nguyenhongthai194@gmail.com (H.Z.N.)
[3] Department of Applied Physics, National University of Kaohsiung, 700, Kaohsiung University Rd., Nanzih District, Kaohsiung 81148, Taiwan; swfeng@nuk.edu.tw
[4] International Medical Center and Department of Chest Medicine, Kaohsiung Armed Forced General Hospital, 2, Zhongzheng 1st.Rd., Lingya District, Kaohsiung City 80284, Taiwan; hweilingchou@gmail.com
* Correspondence: Hsiang-Chen Wang, hcwang@ccu.edu.tw Tel.: +886-5-2729363; Fax: +886-5-2720436

Abstract: InGaN/GaN samples grown on c-plane sapphire substrate with different In concentrations by metal organic chemical vapor deposition are demonstrated. The subsequent capping GaN layer growth opens a possibility for dislocation reduction due to the lateral strain relaxation in growth geometry. We present the further growth optimization and innovative characterization of InGaN layers overgrown on different structures with varying In concentrations. The photoelectrical and optical properties of the InGaN layers with/without capping GaN layer were investigated by time-resolved picosecond transient grating and temperature dependence photoluminescence. We note a 10-fold increase in carrier lifetime in the InGaN layers when the sample structure changes from PIN to single InGaN layer.

Keywords: carrier dynamics; InGaN; four-wave maxing; solar cell; transient grating

1. Introduction

Considering the importance of the worldwide energy demand, the use of photovoltaic devices is widely attractive as an abundant, clean, and renewable energy approach. III-Nitride semiconductors are presently under study as a potential alternative to conventional photovoltaic absorber materials to realize highly efficient solar cells [1-6]. In particular, the entire solar spectrum can be absorbed by the InxGa1-xN system by tuning its direct band gap by optimizing the In composition [7]. Excellent physical properties, such as high mobility, drift velocity, radiation, thermal conductivity, and high temperature resistance leading to long lifetime and strong optical absorption also render InGaN alloys as a possible substitute for conventional solar cell absorbers [7,8]. InGaN-based solar cells also have the potential to be operated under harsh environments, where Si solar cells may suffer from unstable operation [5]. In 2007, Zhang et al. [9] calculated the conversion efficiency of III-nitride photovoltaics in detail and reported an efficiency of up to ~20% from single $In_{0.65}Ga_{0.35}N$ cell. The efficiency can be increased to 35.1% by using InGaN/GaN two junction cells [10]. In the same context, Hsu et al. [11] calculated the efficiency of InGaN/Si tandem solar cells to be increased to 35% when double InGaN junctions are used. Theoretically, the efficiency of multijunction solar cells increases as it incorporates additional junctions and can reach up to 56% for tandem solar cells incorporating eight stack layers [2]. Despite these promising properties, the performances of InGaN-based solar cells still require considerable improvement as most of the reported conversion efficiencies remain low [2,12]. The performance of InGaN-based solar cells is primarily hindered by the structural degradation of thick InGaN layers with high In content (>10%) due to alloy inhomogeneity, vacancy related defects, dislocations, and misfit relaxation [13,14]. To overcome the limitations in thick InGaN layers, researchers have used multiple quantum wells (MQWs) or

superlattice absorbing layers in solar cells because they can limit strain build-up and control defect formation. The improved crystallinity of these MQW structures improves device performances compared with those of solar cells fabricated with thick InGaN absorption layer [2,15,16]. The performance of InGaN MQW-based solar cells can be further improved by increasing the thickness of the active region according to the number of quantum wells [13,17,18]. However, short-circuit current tends to saturate a large number of quantum wells due to carrier collection losses and increased recombination in the MQW region [19]. Therefore, to enhance the photon absorption in InGaN MQWs active region for photovoltaic applications, researchers need to develop new structure or architecture types enabling large InGaN active area.

The nonlinear four-wave mixing (FWM) technique is becoming a versatile tool for the characterization of bulk crystals, as well as semiconductor micro- and nanostructures because it allows the fast and reliable evaluation of novel optoelectronic materials and related technologies. The technique opens a possibility to measure a number of electrical parameters of semiconductors in an "all-optical" way by using well-established correlations between electrical and optical processes. The unique advantage of this technique is the possibility of direct analysis of carrier transport by varying a spacing of light interference pattern. Previous studies on InGaN materials by FWM technique were carried out in heterostructures and single-quantum well samples [20-22]. Okamoto et al. [20] demonstrated that the main reason for the reduction of η_{ext} for a large amount of In is not the increment of nonradiative recombination center but carrier delocalization due to fast diffusion. In our previous work, we presented that the decay times of free carrier gratings with various spatial periods allows the determination of bipolar diffusion coefficient D = 2.1 cm^2/s, effective carrier lifetime of 470 ps, and estimated corresponding hole mobility of 40 cm^2/Vs at carrier density of approximately 10^{18} cm^{-3} [21]. The nonequilibrium carrier dynamics and competition of nonradiative and radiative recombination in differently doped $In_xGa_{1-x}N$ heterostructures have been studied by TR FWM and PL techniques to obtain further insight into the correlation of photoelectric, transport, and structural properties of InGaN alloys [22].

In this study, we optically analyzed InGaN/GaN samples grown on sapphire with different In concentrations and capping layer. The grown structures were evaluated using time-integrated luminescence and time-resolved FWM techniques. In section 2, the growth conditions and experimental procedures are discussed. The X-ray diffraction (XRD), temperature dependence photoluminescence (PL), and time-resolved FWM results are presented in section 3. Finally, the conclusions are drawn in section 4.

2. Sample Structures and Experimental Procedures

In this study, four different $In_xGa_{1-x}N$/GaN samples were grown using metal organic chemical vapor phase deposition. To grow sample SI27, we performed the following steps. First, we purified the sapphire substrate at 1800 °C, applied nitride to the surface, and grew a thin (2 μm) GaN layer at 530 °C. Second, we grew a 200 μm thick layer of $In_{0.27}Ga_{0.73}N$ at 650 °C. Third, we improved the bonding of the $In_{0.27}Ga_{0.73}N$ and GaN layers at 580 °C. CSI27 is a GaN layer with a growth thickness of 120 nm and a growth temperature of 530 °C on SI27. For sample PIN27, the growth steps are as follows. First, we purified the sapphire substrate at 1800 °C, applied nitride to the surface, and grew a thin (1.5 μm) GaN layer at 530 °C. Second, we grew doped Si at 550 °C to form an N-type GaN layer with a thickness of 500 nm. Third, we grew the $In_{0.27}Ga_{0.73}N$ layer at 650 °C. Fourth, we improved the bond between the $In_{0.27}Ga_{0.73}N$ and GaN layers at 580 °C. Fifth, we grew doped Mg at 550 °C to form a P-type GaN layer with a thickness of 120 nm. Sixth, we improved the bond of the $In_{0.27}Ga_{0.73}N$ layer and P-type GaN layers at 580 °C. The growth condition of the sample PIN 15 was similar to that of the sample PIN27, except that the In concentration changed to 15%. The structures of the four samples are shown in Figure 1, as follows:

Preprints (www.preprints.org) | NOT PEER-REVIEWED | Posted: 27 March 2019 doi:10.20944/preprints201903.0253.v1

Peer-reviewed version available at Appl. Sci. 2019, 9, 2279; doi:10.3390/app9112279

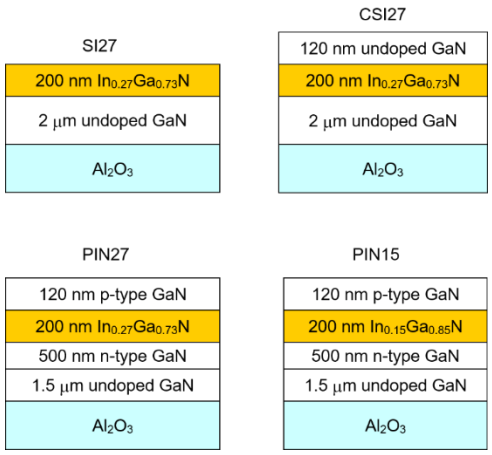

Figure 1. Scheme of InGaN/GaN sample structures used in this work.

Temperature dependence PL measurements were carried out with the 325 nm line of a 50 mW He–Cd laser for excitation. Carrier dynamics in InGaN/GaN samples was investigated using picosecond FWM [23-27]. Time-resolved FWM experiments were carried out using the setup shown in Fig. 2. The measurements of a wide range of materials required different wavelengths for carrier photoexcitation. Therefore, various harmonics of a mode-locked picosecond YAG:Nd laser (model PL2143 of Ekspla Co.) or an optical parametric generator (model PG401 of Ekspla Co.) was used as light sources. The setup provided the pump wavelengths of 532, 355, and 266 nm with the pulse energies of 15, 10, and 5 mJ, respectively. The initial beam diameter was collimated to 1–2 mm in size and used for grating recording. The parametric generator was tunable in the spectral ranges of 420–680 and 740–2000 nm, with the maximum pulse energy of approximately 1 mJ at ~500 nm. In this study, the first harmonic of the laser at 1064 nm was used as a probe beam in most experiments, ensuring the highest sensitivity to the nonresonant refractive index modulation by free carriers. A ps parametric generator at 355 nm as a pump beam was used to record the transient free-carrier grating in the InGaN layer and avoid optical absorption by the GaN layers. The pulse energy of the recording beams was attenuated by rotating $\lambda/2$ plate positioned before the Glan prism. The difference in the optical paths of the interfering beams was adjusted by a short stepper motor-driven pump-delay line that allowed the variation of the delay time of up to 1.5 ns. The energy of the incident beams was measured by an energy meter, whereas the beam spatial profile was controlled by a CCD line. The grating decay kinetics was measured by performing five measurements at a fixed probe beam delay at time Δt and integrating the data in a required intensity window of $I0 \pm \Delta I0$ (generally $\Delta I0/I0 < 5\%$). Exposure characteristics were measured by collecting 500–1000 laser shots at different excitation energies. A data acquisition system on the basis of the LabVIEW software monitored the experiment, processed the data, and presented the measured FWM characteristic in real time. We used the holographic beam splitters (HBSs) to split the pump beam as two beams to form a dynamic grating in the sample. A simple temporal and spatial adjustment of two interfering beams created by the HBS and easy change of the dynamic grating period by replacing only the HBS with another grating of a different spacing makes the novel FWM tool user-friendly, reproducible, and simple in operation. The experimental set-up is shown in Fig. 2. θ is the angle between two incident beams of the pump beam. A reference paper [28] showed additional details about this nondegenerate ps FWM by using HBS component. The free-carrier grating through the excitation of a crystal with light interference patterns shows some advantages over other excite-probe techniques. These advantages were due to the temporal and spatial modulation of optical properties of a matter by incident light $I(x) = I0$

Preprints (www.preprints.org) | NOT PEER-REVIEWED | Posted: 27 March 2019 doi:10.20944/preprints201903.0253.v1

Peer-reviewed version available at Appl. Sci. 2019, 9, 2279; doi:10.3390/app9112279

[1+cos(Kx)], which generated a spatially modulated nonequilibrium carrier distribution N(x,t) = N0(t) +ΔN(x,t) cos(Kx), where N0 and ΔN are the non-modulated and modulated carrier densities along the grating vector K = 2π/Λ with period Λ, respectively. The instantaneous modulation of the electric properties is duplicated by the refractive index n modulation by value Δn(x,t) ~ ΔN(x,t), thereby creating a free carrier grating [29]. The decay time of the grating efficiency η(t) ~ $\exp(-\Delta t/\tau_G)$ corresponded to the time interval of the probe beam $\Delta t = \tau_G$, in which the η value decreased by e2, while carrier modulation decreased by e in this interval. The similar procure was repeated at some other grating periods, and the corresponding values of τ_G were determined. The plot of the inverse grating decay time $1/\tau_G$ versus $(2\pi/\Lambda)^2$ (or the so-called angular dependence of decay time) allowed the determination of the diffusion coefficient, as well as the carrier recombination time, because one of them is dependent on grating period, as follows.

$$\frac{1}{\tau_G} = \frac{1}{\tau_R} + \left(\frac{2\pi}{\Lambda}\right)^2 D \qquad (1)$$

where $1/\tau_R$ is the recombination time, and $\tau_D = \Lambda 2/(4\pi 2D)$ is the diffusion time of the grating erasure.

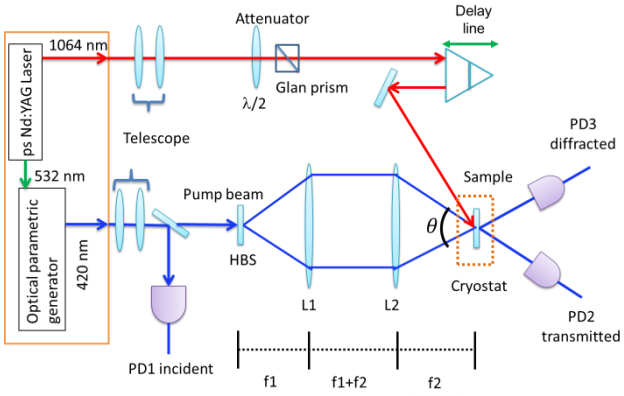

Figure 2. Optical scheme of nondegenerate four-wave mixing with HBS as the beam splitter.

3. Results and Discussions

3.1 Band Gap of InGaN

Knowing that the energy gap of InGaN varies with the In concentration is necessary for the design of an InGaN-based optical power supply to obtain high-efficiency luminescence with a target light wavelength from the InGaN layer. The change in the InGaN energy gap with In concentration is also an important issue in theoretical research. Unfortunately, the light emission of InGaN is not from a uniform InGaN layer but from a local structure due to In segregation, phase separation, and other reasons. These phenomena make the PL emission much lower than the energy gap of the "carrier" InGaN layer and unusable in obtaining the InGaN energy gap. The most common methods used in the literature to measure the energy gap of InGaN are absorption spectra [30, 31], optical density measurements [32], and PL excitation spectra [33, 34]. A discussion of the energy gap bending parameters of InxGa1-xN as a function of x is underway. Given the difficulty of the high In concentration growth of InGaN and pure In, the energy gap of InxGa1-xN with high x or x = 1 is rarely studied. Thus, the uncertainty of the energy gap with a high In concentration must be studied. Given the improved growth of h-InN, the effects of O and interfacial metal clusters can be avoided [35]. The InN energy gap has been measured and discussed in several papers. The new h-InN energy gap was in the range of 0.7–1.4 eV. Bechstedt et al. [36] calculated the InN energy gap, which is 0.58

Preprints (www.preprints.org) | NOT PEER-REVIEWED | Posted: 27 March 2019 doi:10.20944/preprints201903.0253.v1

Peer-reviewed version available at Appl. Sci. 2019, 9, 2279; doi:10.3390/app9112279

eV. The sample we studied was an InGaN layer grown on a GaN buffer layer by using a sapphire (Al_2O_3) substrate. The energy gap of InGaN and In concentration was determined using the following equation (Equation [2]) according to the reference [37]:

$$Eg_{(x)} = 0.7x + 3.4(1 - x) - 1.43x(1 - x). \quad (2)$$

3.2. XRD Results

Figure 3 shows an ω-2θ line scan with different InxGa1-xN layers grown on a sapphire (Al_2O_3) substrate. The peak with the greatest intensity is the Bragg reflection from the GaN buffer layer, whereas the arrows in the figure represent the InxGa1-xN peaks of the four samples (i.e., SI27, CSI27, PIN15, and PIN27). SI27 exhibited a diffraction signal of $In_{0.27}Ga_{0.73}N$ at 33.56°. The sample CSI27 showed a diffraction signal of $In_{0.48}Ga_{0.52}N$ and $In_{0.19}Ga_{0.81}N$ at 32.92° and 33.80°, respectively. PIN27 had the diffraction signals of $In_{0.47}Ga_{0.53}N$ and $In_{0.2}Ga_{0.8}N$ at 32.94° and 33.78°, respectively. PIN15 exhibited a diffraction signal of $In_{0.15}Ga_{0.85}N$ at 34.05°, while CSI27 and PIN27 produced two different crystal phases of InxGa1-xN. The possible reason for this finding is that the concentration of doped In was extremely high. Hence, the concentration of a part of In was diffused into the uppermost layer of GaN, thereby resulting in two different crystal phases of InxGa1-xN. Table 1 presents the XRD measurement results of SI 27, CSI27, PIN27, and PIN15 according to Equation (7). The InGaN peak shown in Figure 3 exhibited an increased distance from the GaN peak. All InGaN layers were characterized by pseudomorphicity on the GaN buffer layer. CSI27 and PIN27 exhibited two separate InxGa1-xN phase peaks detected from the InGaN/GaN scan in Figure 3. The tilt of the InGaN layer to the GaN buffer layer was not found in the four samples studied.

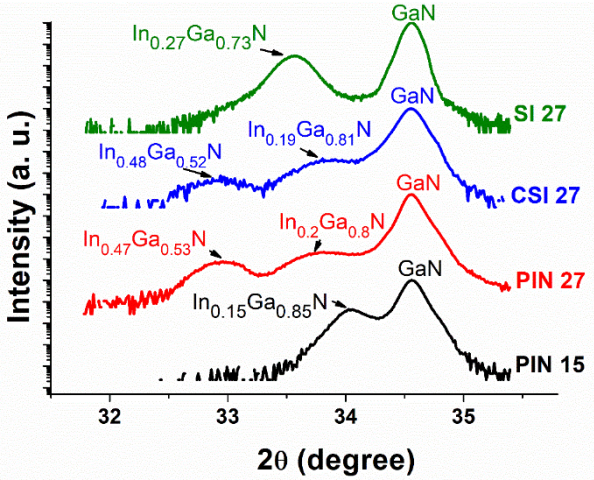

Figure 3. XRD results of four samples.

Table 1. Relationship between the In concentration of $In_xGa_{1-x}N$ and energy bap

InGaN	Eg (eV)
$In_{0.27}Ga_{0.73}N$	2.389
$In_{0.48}Ga_{0.52}N$	1.747
$In_{0.19}Ga_{0.81}N$	2.667
$In_{0.47}Ga_{0.53}N$	1.775
$In_{0.2}Ga_{0.8}N$	2.631
$In_{0.15}Ga_{0.85}N$	2.813

3.3. PL Results

Figure 4 shows the temperature-dependent PL spectra of the samples. In SI27 (Fig. 4[a]), the temperature-dependent PL peak energy did not exhibit an S-shape behavior. The S-shape behavior has been attributed to the carrier dynamics associated with carrier localization in potential minimums [23-25, 38, 39]. As shown in Fig. 4(b), two PL spectral peaks were identified below 150 K. The low-energy peak corresponded to the localized states. The high-energy peak was attributed to the free-carrier states, corresponding to the background InGaN compound on which clusters were distributed. However, the background InGaN compound also consisted of the potential fluctuations of shallow distributions. The merging of the two PL peaks above 150 K was attributed to carrier liquidation among the localized states and free-carrier states. The decreasing trend of the high-energy peak was mainly due to the band-gap shrinkage of phonon effect [40]. As shown in Fig. 4(c), the PL peaks showed broader bandwidth than that of the SI27 sample, which indicated that the In concentration fluctuation was evident. As shown in Fig. 4(d), the PL peak position corresponded to low In concentration (~15%). The optical quality of PIN15 was poor due to the low emission energies existing between 450 and 500 nm.

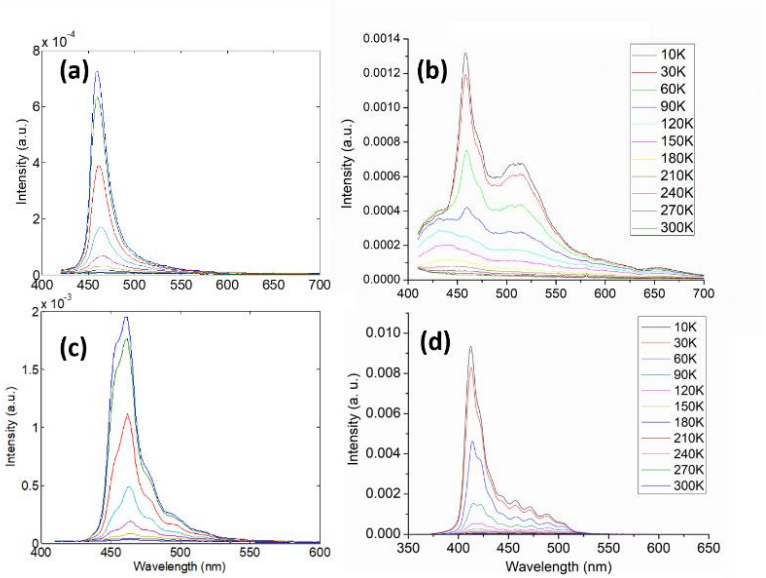

Figure 4. Temperature dependence PL spectra of the samples (a) SI27, (b) CSI27, (c) PIN27, and (d) PIN15.

3.4. Time-resolved FWM Results

The measurements were carried out at room temperature with various excitation energy densities I. The decay of LITG recorded in the samples is shown in Fig. 5. The decay kinetics was nearly exponential and fast for small grating periods, which was in accordance with Equation (1). The τR and D values were determined by plotting the dependence of grating decay rate 1/τG versus inverse grating period ΔN-2. Similarly, we measured the grating decay rates in InGaN layers grown on different In concentrations. The determined parameters are presented in Table II. The data indicated that the lifetime decreased with excitation energy densities. CSI27 and PIN27 had the longest carrier lifetimes and typical D values for InGaN. The complementary measurements of PL intensity at 325 nm excitation (Fig. 4) demonstrated the increased radiative recombination component due to decreased nonradiative recombination rate in InGaN layers. The presence of a high density of defects in the used template may also influence the quality of the InGaN layers. The extremely short carrier lifetime of ~150 ps that was observed in the PIN27 and its ~10-fold increase with excitation reflected the high defect density and partial saturation of electron trapping centers by the injected

Preprints (www.preprints.org) | NOT PEER-REVIEWED | Posted: 27 March 2019 doi:10.20944/preprints201903.0253.v1

Peer-reviewed version available at Appl. Sci. 2019, 9, 2279; doi:10.3390/app9112279

carriers. In CSI27, four power measurement results were provided, thereby showing better quality than the other samples.

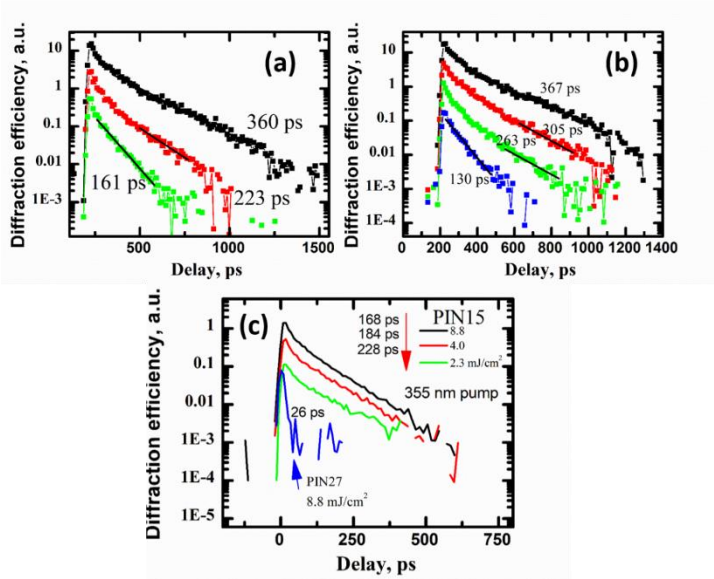

Figure 5. FWM decay spectra with different excitation powers on (a) SI27, (b) CSI27, (c) PIN15, and PIN27, with the excitation powers of 8.8, 4.0, 2.3, and 1.5 mJ/cm², respectively.

Table 2. Carrier lifetime τ_R (ps) and diffusion coefficient D (cm²/s) in InGaN layers grown on different In concentrations (SI27, CSI27, PIN27, and PIN15).

Sample / I_0 (mJ/cm²)	SI 27 (cm²/s, ns, ps)			CSI 27 (cm²/s, ns, ps)			PIN27 (cm²/s, ns, ps)			PIN 15 (cm²/s, ns, ps)		
	D_a	τ_R	τ_G	D_a	τ_R	τ_G	D_a	τ_R	τ_G	D_a	τ_R	τ_G
8.8	1.73	1.48	360	1.83	1.59	367	2.73	0.15	26	2.56	0.45	228
4.0	1.60	1.35	223	1.74	1.33	305				2.32	0.42	184
2.3	1.23	1.22	161	1.53	1.25	263				2.08	0.31	168
1.5				1.28	1.05	130						

4. Conclusion

Using complementary optical techniques, we confirmed the improved electrical, optical, and structural parameters of InGaN layers on different In concentrations. A carrier lifetime of 1.59 ps and diffusion coefficient D of 1.83 cm²/s was optimal for CSI27. Sample quality increased in the capping GaN epilayer when the In concentration was 27%. This feature indicated an approximately twofold decrease in defect density. Low-efficiency electron trapping in the overgrown GaN was supported by the D = 1.6 cm²/s value, which was typical for bipolar plasma in GaN, whereas the D value was two times faster in the template (as n < p). Increasing lifetime value with excitation was typical for the saturation of electron trapping centers by excess carriers in InGaN with capping GaN structure.

Acknowledgments: This research was supported by the Ministry of Science and Technology, the Republic of China (grant no. MOST 106-2112-M-194-002) and Kaohsiung Armed Forces General Hospital research project 104-43.

This work was financially/partially supported by the Advanced Institute of Manufacturing with High-Tech Innovations from the Featured Areas Research Center Program within the framework of the Higher Education Sprout Project by the Ministry of Education in Taiwan.

Author Contributions: Zhi Ting Ye and Hong-Thai Nguyen were responsible for data and optical measurements. Zomg-Zhan Li analyzed the XRD PL and FWM results. Shih-Wei Feng, Zhi Ting Ye, Hwei-Ling Chou, and Hsiang-Chen Wang organized and wrote the manuscript.

Conflicts of Interest: The authors declare no conflict of interests.

References

1. J. J. Wierer, Q. Li, D. D. Koleske, S. R. Lee and G. T. Wang, *Nanotechnology*, **2012**, *23*, 194007.
2. A. G. Bhuiyan, K. Sugita, A. Hashimoto and A. Yamamoto, *IEEE J. Photovolt*., **2012**, *2*, 276–293.
3. R. Dahal, J. Li, K. Aryal, J. Y. Lin and H. X. Jiang, *Appl. Phys. Lett*., **2010**, *97*, 73115.
4. M. Mori, S. Kondo, S. Yamamoto, T. Nakao, M. Iwaya, T. Takeuchi, S. Kamiyama, I. Akasaki and H. Amano, *Jpn. J. Appl. Phys*., **2013**, *52*, 08JH02.
5. D. H. Lien, Y. H. Hsiao, S. G. Yang, M. L. Tsai, T. C. Wei, S. C. Lee and J. H. He, *Nano Energy*, **2015**, *11*, 104–109.
6. B. O. Jung, S. Y. Bae, S. Y. Kim, S. Lee, J. Y. Lee, D. S. Lee, Y. Kato, Y. Honda and H. Amano, *Nano Energy*, **2015**, *11*, 294–303.
7. J. Wu, W. Walukiewicz, K. M. Yu, W. Shan, J. W. Ager, E. E. Haller, H. Lu, W. J. Schaff, W. K. Metzger and S. Kurtz, *J. Appl. Phys*., **2003**, *94*, 6477–6482.
8. G. Meneghesso, G. Verzellesi, F. Danesin, F. Rampazzo, F. Zanon, A. Tazzoli, M. Meneghini and E. Zanoni, *IEEE Trans. Device Mater. Reliab*., **2008**, *8*, 332–343.
9. X. Zhang, X. Wang, H. Xiao, C. Yang, J. Ran, C. Wang, Q. Hou and J. Li, *J. Phys. D: Appl. Phys*., **2007**, *40*, 7335–7338.
10. X. Zhang, X. Wang, H. Xiao, C. Yang, J. Ran, C. Wang, Q. Hou, J. Li and Z. Wang, *J. Phys. D: Appl. Phys*., **2008**, *41*, 245104.
11. L. Hsu and W. Walukiewicz, *J. Appl. Phys*., **2008**, *104*, 024507.
12. O., Jani, I. Ferguson, C. Honsberg and S. Kurtz, *Appl. Phys. Lett*., **2007**, *91*, 132117.
13. N. G. Young, R. M. Farrell, Y. L. Hu, Y. Terao, M. Iza, S. Keller, S. P. Denbaars, S. Nakamura and J. S. Speck, *Appl. Phys. Lett*., **2013**, *103*, 173903.
14. N. G. Young, E. E. Perl, R. M. Farrell, M. Iza, S. Keller, J. E. Bowers, S. Nakamura, S. P. Denbaars and J. S. Speck, *Appl. Phys. Lett*., **2014**, *104*, 163902.
15. Y. Kuwahara, T. Fujii, T. Sugiyama, D. Iida, Y. Isobe, Y. Fujiyama, Y. Morita, M. Iwaya, T. Takeuchi, S. Kamiyama, I. Akasaki and H. Amano, *Appl. Phys. Express*, **2011**, *4*, 21001.
16. K. Y. Lai, G. J. Lin, Y. L. Lai, Y. F. Chen and J. H. He, *Appl. Phys. Lett*., **2010**, *96*, 81103.
17. S. Valdueza-felip, A. Mukhtarova, Q. Pan, G. Altamura, L. Grenet, C. Durand, J. Eymery, E. Monroy, C. Bougerol, D. Peyrade and F. Gonza, *Jpn. J. Appl. Phys*., **2013**, *52*, 08JH05.
18. N. Watanabe, M. Mitsuhara, H. Yokoyama, J. Liang and N. Shigekawa, *Jpn. J. Appl. Phys*., **2014**, *53*, 112301.

19. A. Mukhtarova, S. Valdueza-Felip, L. Redaelli, C. Durand, C. Bougerol, E. Monroy and J. Eymery, *Appl. Phys. Lett*., **2016**, *108*, 161907.

20. K. Okamoto, A. Kaneta, K. Inoue, Y. Kawakami, M. Terazima, G. Shinomiya, T. Mukai, and Sg. Fujita, *Phys.stat.sol*., **2001**, *(b) 228*, 81.

21. R. Aleksiejunas, M. Sudžius, V. Gudelis, T. Malinauskas, K. Jarašiunas, Q. Fareed, R. Gaska, M. S. Shur, J. Zhang, J. Yang, E. Kuokštis, and M. A. Khan, *Phys. stat. sol*., **2003**, *(c) 7*, 2686.

22. K. Jarasiunas, R. Aleksiejunas, T. Malinauskas, S. Miasojedovas, S. Jursenas , A. Zukauskas, R. Gaska, J. Zhang, M. S. Shur, J. W. Yang, E. Kuokstis, M. A. Khan, *Phys. stat. sol*., **2005**, *(a) 202*, 820.

23. Hsiang-Chen Wang, Xuan-Yu Yu, Yu-Lun Chueh, Tadas Malinauskas, K. Jarasiunas, and Shih-Wei Feng, "Suppression of surface recombination in surface plasmon coupling with an InGaN/GaN multiple quantum well sample," *Optics Express*, **2011**, 19-18893.

24. Hsiang-Chen Wang, Tsung-Yi Tang, C. C. Yang, T. Malinauskas , K. Jarasiunas. Carrier dynamics in coalescence overgrowth of GaN nanocolumns. *Thin Solid Films*, **2010**, 519, 863.

25. Hsiang-Chen Wang, T. Malinauskas , K. Jarasiunas, Shih-Wei Feng, Chu-Chi Ting , Sean Liu. Carrier dynamics in InGaN/GaN multiple quantum wells based on different polishing processes of sapphire substrate. *Thin Solid Films*, **2010**, *518*, 7291.

26. T. Malinauskas, R. Aleksiejunas, K. Jarašiunas, B. Beaumont, P. Gibart, A. Kakanakova-Georgieva, E. Janzen, D. Gogova, B. Monemar, M. Heuken, *J. Cryst. Growth*, **2007**, *300*, 223.

27. K. Jarasiunas, R. Aleksiejunas, T. Malinauskas, V. Gudelis, T. Tamulevicius, S. Tamulevicius, A. Guobiene, A. Usikov and V. Dmitriev, and H. J. Gerritsen, *Rev. Sci. Inst*., **2007**, *78*, 033901.

28. K. Jarasiunas, R. Aleksiejunas, T. Malinauskas, V. Gudelis, T. Tamulevicius, S. Tamulevicius, A. Guobiene, A. Usikov and V. Dmitriev, and H. J. Gerritsen. Implementation of diffractive optical element in FWM scheme for ex situ characterization of hydride vapor phase epitaxy-grown GaN layers. *Rev. Sci. Inst*., **2007**, *78*, 033901.

29. M. Syvajarvi, R. Yakimova. Wide Band Gap Materials and New Developments. *Research Signpost*, **2007**.

30. J. Wu, W. Walukiewicz. Superlattices and Microstructures, **2003**, *34*, 63.

31. T. Matsuoka, H. Okamoto, M. Nakao et al., *Appl.Phys.Lett*., **2002**, *81 (7)*, 1246.

32. M. Ryu, E. Kuokstis, C. Chen, J. Yang, G. Simin, M. Khan, G. Sim, and P. Yu, *Solid state commun*., **2003**, *126*, 329.

33. M.E. White, K.P. O'Donnell, R.W. Martin et al., *Mater. Sci. Eng*., **2002**, *B 93*, 147.

34. S.F. Li, D.J. As, K. Lischka et al., *Mater. Res. Soc. Symp. Proc*., **2005**, *831*, E8.15.1.

35. M. P. Halsall, J. E. Nicholls, J. J. Davies, B. Cockayne, P. J. Wright, *J. Appl.Phys*., **1992**, *71 (2)*, 15.

36. F. Bechstedt, J. Furthmüller, M. Ferhat et al., *Phys.stat.sol*., **2003**, *(a) 195 (3)*, 628.

37. Vaitkus, S., Jarasiunas, K., Gaubas, E., Jonikas, L., Pranaitis, R., and Subacius, L., *IEEE J. Quant. Electr*., **1986**, *QE-22*, 1298.

38. Y. H. Cho, G. H. Gainer, A. J. Fischer, J. J. Song, S. Keller, U. K. Mishra, and S. P. DenBarrs, *Appl. Phys. Lett*., **1998**, *73*, 1370.

39. P. G. Eliseev, P. Perlin, J. Lee, and M. Osinski, *Appl. Phys. Lett*., **1997**, *71*, 569.

40. Hsiang-Chen Wang, Yen-Cheng Lu, Chih-Chung Teng, Yung-Sheng Chen, C. C. Yang, Kung-Jen Ma, Chang-Chi Pan and Jen-Inn Chyi. Ultrafast Carrier Dynamics in an InGaN Thin Film. *J. Applied Physics*, **2005**, *Vol. 97, No. 3*, pp. 033704-1-4.